N96-15559

THE EFFECTS OF SOOTING IN DROPLET COMBUSTION

Kyeong-Ook Lee, Kirk Jensen and Mun Young Choi
Department of Mechanical Engineering
University of Illinois at Chicago
Chicago, IL 60607

1.0 INTRODUCTION

The study of the burning of a single droplet is an ideal problem from which to gain fundamental understanding of diffusion flame characteristics. Droplet combustion is a complex physico-chemical process that involves a chemically-reacting two-phase flow with phase changes and yet simple experiments and analysis can be used to attain important insights into the burning rate, flame dynamics, kinetic extinction and disruption processes. It is a subject that has been actively studied for the past 40 years with most of the fundamental experiments being performed under reduced-gravity conditions for direct comparisons with theoretical/computational analyses that invoke spherical symmetry assumptions.

In the earlier studies, the effects of sooting on the overall burning characteristics were not considered [Kumagai and Okajima, 1957; Kumagai, Sakai and Okajima, 1971]. However, recent microgravity investigations performed at the NASA-LeRC droptowers **(Droplet Combustion Experiment of Professor F.A. Williams and Professor F.L. Dryer)** and others indicate that effects of soot and sootcloud formation may be significant during the lifetime of the droplet and therefore must be included in the analysis [Knight and Williams, 1980; Shaw et al., 1988; Choi et al., 1990; Jackson et al., 1991; Avedisian, 1994].

1.1 Droplet Burning Rate

Sooting mechanisms can have profound effects on the overall droplet burning rate. In an earlier study on microgravity n-heptane droplet combustion experiments, vaporization rates that were as much as 30% to 40% lower than the classically-accepted results were reported [Choi et al., 1990]. The main conclusion drawn from that investigation was that the effects of formation and accumulation of the sootshell and its asymmetric configuration caused by small degrees of relative droplet/gas convection were responsible for the observed discrepancies. There are several mechanisms through which soot/sootshell formation can affect the burning rate. Soot formation is an endothermic process and will act as a heat sink for the energy that would otherwise be used to vaporize the fuel. Although, exact figures for the conversion to soot is not presently known for microgravity droplet combustion, results from normal gravity pyrolysis experiments suggest relatively large conversion rates ~ 30% [Vranos and Liscinsky, 1984]. Furthermore, heat loss at the flame due to soot radiation can reduce the effective transfer number by decreasing the amount of energy available to vaporize the fuel. Related to these phenomena is the accumulation of the formed soot in the region bounded by the droplet and the flame. This represents unrealized chemical energy resulting in the reduction of the heat of combustion available from the vaporized fuel.

1.2 Extinction

Analysis of the extinction mechanism during droplet combustion is important for extracting overall chemical kinetic rates for large hydrocarbons for which detailed information does not exist [Chung and Law, 1986; Williams and Dryer, 1994]. Extinction occurs when the flow time of the reactants becomes smaller than the time needed for the reactants to be consumed (when the Dahmkohler number is reduced below a critical value). The critical Dahmkohler number is given by where d_{ext} is the extinction diameter, D_g is the diffusivity and t_c is the characteristic chemical reaction time.

$$Da_{cr} = \frac{d_{ext}^2/D_g}{t_c} \qquad (1)$$

However, extinction can occur prematurely if radiative losses from the flame decreases the flame temperature and therefore affect the chemical reaction time. Chao and coworkers [Chao et al., 1990] suggest that radiative losses from the flame can promote the onset of kinetic extinction. For droplet flames that produce soot, it is likely that soot radiation will dominate and therefore affect the kinetic extinction process [Grosshandler, 1992]. Thus far, only a limited number of extinction measurements have been reported for n-heptane droplets burning in air [Yang and Avedisian, 1988; Hara and Kumagai, 1990]. However, the extinction diameter is usually very small and not always reproducible under mildly sooting conditions. Without accurate determination of the soot concentration near the flame, it is not known to what degree soot formation may eventually affect droplet extinction.

1.3 Disruptive Burning

In a previous work by Knight and Williams [1980], disruption was observed during the combustion of alkane droplets in a microgravity environment. Disruption is a process by which the original droplet is violently shattered and burns as smaller satellite droplets. In subsequent experiments in the NASA-Lewis droptower [Shaw et al., 1988], it was found that the likelihood of observing the disruption behavior was higher for fuels (and or conditions such as higher oxygen concentrations) that produced high soot loading.

Shaw and Williams [1990] presented results that suggest that the absorption of heavy soot precursors on the droplet surface can create conditions in which an outer layer (of soot precursors) can reach temperatures exceeding the superheat temperature of the original fuel. Another possible mechanism suggests that the soot particles can come in contact with the droplet and cause rapid heating. Although a definitive explanation does not exist, it is clear that the sooting mechanism is very important in the disruptive burning process.

1.4 Thermophoresis

For droplet combustion, soot particles form in the fuel-rich region of the diffusion flame through pyrolysis reactions. These reactions are high-activation energy processes and thus maximum soot production will likely occur near the flame [Shaw et al. 1988]. Once soot is formed in the fuel-rich region, they are acted upon by viscous drag (caused by Stefan flow) and Thermophoresis. Thermophoresis is a mechanism through which particle transport is caused by a temperature gradient in the surrounding gas-phase [Friedlander, 1977]. Waldmann and Schmitt [1966] analyzed the viscous drag and thermophoretic force acting on a small spherical particle by calculating the momentum transferred per unit time to the particle by the impinging and rebounding gas molecules. At equilibrium [$\sum F$ is equal to 0], these two forces are balanced. The resulting equation can then be solved for the flux, ρV_t.

$$\rho V_t = \frac{-3\mu dT/dr}{4(1+\pi\alpha/8)T} = g(r) \qquad (2)$$

The term, ρV_t is defined as the thermophoretic flux. The thermophoretic flux is the convective flux necessary for the above-mentioned force equilibrium on the particle to be maintained.

Opposing the thermophoretic forces is the viscous drag caused by the Stefan flux, where (dm/dt) is the droplet mass gasification rate.

$$\rho V_r = \frac{dm/dt}{4\pi r^2} \qquad (3)$$

Eqn. 3 is valid under conditions of negligible surface regression rate compared to the gas velocity at the surface which is satisfied when the ratio of the liquid to gas densities is large. The sootshell will form at the radial position where the viscous drag and thermophoretic forces are in balance.

The above formulation is valid for soot particles that are much smaller than the mean free path. Jackson and coworkers [1991] implemented the thermophoretic model of Talbot and coworkers [1980]. In this model, the sootshell location can be calculated by assuming the soot particle dimension. Therefore, the measurement of the characteristic dimensions of the soot particles (including the radius of gyration and primary particle size using thermophoretic sampling and TEM) will be important in comparing the experimental and theoretical sootshell locations.

1.5 Droplet Flame Dynamics

The flame diameter is also affected by the soot formation through reductions in the specific volume [Choi et al., 1993]. After the initial period of fuel vapor accumulation (during which fuel vapor fills the increasing volume between the droplet surface and the flame front), quasi-steady conditions should exist under which the gasified mass will equal the mass consumed at the flame front. However, under sooting conditions, portions of the gasified fuel are converted to soot (which possess negligible specific volume when compared to that of the gaseous species). Therefore, soot accumulates in the sootshell and never reaches the flame front.

2.0 The Need for Accurate Measurement of Soot Volume Fraction and Temperature

Since the pioneering microgravity droplet combustion experiments of Kumagai and coworkers back in 1957, there have been numerous theoretical, computational and experimental studies analyzing the burning characterstics of isolated droplets. In all subsequent microgravity droplet combustion studies, the degree of sooting was estimated by visual observations of the sootshell. This practice could not provide detailed information regarding the transient distribution of the soot and temperature in the region bounded by the flame and the droplet. For all of the important parameters of interest in droplet combustion including the variations in the

burning rate, promotion of extinction, reduction in flame size, onset of disruptive burning and soot dynamics, it is clear that accurate measurements of the degree of sooting and the temperature field within the region bounded by the droplet and the flame is needed to further advance our understanding.

In the present study, the sooting behavior will be studied using light extinction measurements and Abel deconvolution to determine the radial distribution of soot volume fraction; two-wavelength optical pyrometry to determine the soot temperature within the region between the flame and the droplet; and thermophoretic sampling/transmission electron microscopy to determine the soot morphology (radius of gyration and primary particle size). In addition, computational modeling [using the Chemically-Reacting-Flow-Model of Princeton] of the soot particle dynamics involving the balance between thermophoresis and Stefan drag will be compared with the experimental measurements. The modeling efforts will be advanced interactively with the experimental measurements of the soot volume fractions and the soot particle dimensions.

These experiments will be performed for a wide range of conditions to vary the sooting propensity of the droplet using various fuels (including decane, heptane, toluene/methanol mixtures, benzene/methanol mixtures and ethanol etc.), pressure (0.1 to 1.0 atm), oxygen indices (0.15 to 0.50), initial droplet diameters (1.0 to 5.0 mm) and inerts (N_2, He, CO_2, etc.) as parameters.

3.0 EXPERIMENTAL APPROACH

3.1 Soot Volume Fraction Measurements

Kadota and Hiroyasu [1984] first measured soot concentration in droplet flames using optical techniques. In their study, light extinction measurements were performed at a fixed location below the droplet and the radial variation was deduced by assuming that the regressing flame maintained constant spherical structure. This procedure may produce realistic information since the flame geometry is nearly spherical in the region below the droplet. However, the same approach will produce unrealistic results in the region above the flame where it displays both axial and radial variations.

In the present experiment, the soot volume fraction will be measured using a full-field light extinction technique that was developed at **NASA-Lewis Research Center** by **Greenberg, Griffin and Ku** [Griffin and Greenberg, 1992; Greenberg and Ku, 1995] for eventual use in measuring the soot volume fraction for microgravity droplet combustion. Feasibility of this technique was investigated by performing soot volume fraction measurements for suspended droplets burning under normal-gravity conditions.

Fig. 1 displays the schematic of the experimental apparatus similar to the system of Greenberg and Ku [1995]. Light from the HeNe laser is first passed through a variable neutral density filter and expanded through a spatial filter/collimator to produce a 50mm diameter beam. The beam is directed through opposing optical ports (each fitted with 51mm diameter quartz windows) of the stainless steel droplet combustion chamber. The transmitted beam is imaged using a high-resolution CCD camera (with attached interference and neutral density filters). The entire burning history is recorded onto a S-VHS recorder and subsequently the image is digitized frame-by-frame using a high-resolution (512x480 pixels) data acquisition board. Measurements indicate that the laser/detection system is very stable with temporal fluctuations of the light intensity less than 0.5% of the total magnitude of the intensity.

For the normal-gravity droplet combustion experiment, a single droplet of 2mm diameter is deposited on a bead that is formed at the end of the suspending quartz fiber (diameter is approximately 150 micrometers) using a hypodermic needle. The orientation of the fiber as shown in inset A in fig. 1 was designed to minimize interactions with the burning by reducing its contact with the flame (For the proposed microgravity experiment, droplets will be suspended by using cross-hairs of 50 micron silica carbide fibers). The droplets are ignited using an induction coil discharge igniter.

For each horizontal plane, the line of sight projection data, $P_{f_v}(x)$, is given by:

$$P_{f_v}(x) = \int_{-\infty}^{\infty} f_v \sqrt{(x^2+y^2)}\,dy \qquad (4)$$

The Abel transform allows the calculation of the field distribution $f_v(r)$ corresponding to the projection data with the underlying assumption that it is radially symmetric [Santoro et al., 1983; Dasch, 1992; Sunderland et al., 1995]. The soot volume fraction distribution (based on extinction) is found from the measured transmission of each projection:

$$\tau_\lambda(x) = \frac{I_\lambda}{I_{\lambda o}}(x) = \exp\left[-\frac{K_e}{\lambda}\int_{-\infty}^{\infty} f_v \sqrt{(x^2+y^2)}\,dy\right] \qquad (5)$$

where K_e is the dimensionless extinction constant of soot. In this study, K_e value of 8.8 which was measured for soot in the post-flame region of a rich acetylene flame was used [Choi et al., 1995]. Equation 5 can be rearranged into the form of the projection value as:

$$P_{f_v}(x) = -\frac{\lambda}{K_e}\ln\left(\frac{I_\lambda}{I_{\lambda o}}\right) = \int_{-\infty}^{\infty} f_v \sqrt{(x^2+y^2)}\,dy \qquad (6)$$

For a typical experiment, nearly 200 images are produced, therefore, full-field determination of the soot volume fraction measurements requires the analysis of more than 30,000 projection data files. To increase the efficiency, a full-field algorithm was written to analyze the entire experiment [Greenberg and Ku, 1995 have also written a similar algorithm].

In the present study, the soot volume fraction is measured as a function of radial position for hydrocarbon mixture flames at various heights above the droplet. Figure 2 displays the resulting G/G_o (where G corresponds to graylevel) profiles for t = 2 sec after ignition. The entire image is filtered using a 3x3 low-pass filter and the individual vertical position data is 5-pt averaged. The horizontal axis corresponds to the column position and the vertical axis corresponds to row positions. The maximum attenuation is approximately equal to 0.4. From this profile, the soot volume fraction is determined using the full-field Abel-deconvolution algorithm [See fig. 3]. A curve-fitting algorithm is used to define the center of the sooting region for each vertical position and the soot volume fraction on either side of the center is averaged to obtain the final output. The soot volume fraction increases from as a function of height and radial position from the center. The soot volume fraction is maximum near the flame at all vertical locations which is consistent with the structure of diffusion flames.

3.2 Soot Temperature Measurement Technique

The temperature of the soot particles within the region between the droplet surface and the flame front will be measured using a two-wavelength pyrometry and Abel deconvolution [Faeth, 1994]. The emission from the flame will be simultaneously directed to two separate CCD cameras (with a narrow bandpass filters at 800 nm and 900 nm) using a beamsplitter. Due to the small size of soot particles, the discrepancy with the local gas temperatures is expected to be small [Köylü and Faeth, 1993]. The emission intensity at each central wavelength measured for a vertical plane corresponds to the projection value of the integrated emission.

$$P_{I_\lambda}(x) = \int_{-\infty}^{\infty} K_\lambda I_{b\lambda}\,dy \qquad (7)$$

$$K_\lambda = \frac{36\pi nk}{(n^2 - k^2 + 2)^2 + 4n^2k^2}\frac{f_v}{\lambda} \qquad (8)$$

where $I_{b\lambda}$ is Planck's function. The projections values for 800 nm and 900 nm can be deconvoluted separately using the Abel technique to determine the corresponding product of $(K_\lambda I_{b\lambda})$ as a function of radial position. The ratio of the emission at 800 nm and 900 nm can then be used to determine the temperature using the two-wavelength pyrometry formula [Sivathanu and Faeth, 1990].

3.3 Soot Morphology Measurement Technique

The morphology of soot aggregates will be determined by performing thermophoretic sampling experiments [Megaridis and Dobbins, 1988]. Thin ribbons of copper mesh grids will be rapidly inserted into the flame to obtain instantaneous distribution of soot morphology. Temporal variation of the soot will be determined by inserting different ribbons at pre-determined times. Subsequent analyses will involve obtaining transmission electron micrographs and analyzing the radius of gyration using a non-subjective digital image processing technique that was developed as part of this project [Choi and Zhou, 1995].

4.0 PROGRESS TO DATE

a) A droplet combustion chamber which utilizes several features of the DCE droptower hardware is being fabricated at NASA-LeRC to take advantage of the design solutions. The UIC team will incorporate all of the optical diagnostic equipment to the experimental package. It is anticipated that an operational soot volume fraction/temperature rig to be used in the DC-9 and in the 2.2 sec droptower will be ready by mid-summer of 1995.

b) A full-field normal-gravity droplet combustion apparatus to perform soot volume fraction measurements was implemented at UIC. Performed experiments using various hydrocarbon mixture droplets.
(results will be presented at the Central States Sectional Meeting of the Combustion Institute, 1995).

c) Developed an interactive Abel-deconvolution algorithm to determine soot volume fraction for full-field light extinction data. This program manipulates the full-field digitized image data and produces the I/Io information at every single pixel location. The information is then used to determine the soot volume fraction information for each horizontal plane.

Similar program was also written for two-wavelength pyrometry.

d) Developed a digital image processing program to determine the radius of gyration from transmission electron micrographs. The students are fully trained in TEM and Selected Area Electron Diffraction Techniques.

e) Submitted a proposal (with P. Ferkul and D. Schultz of NASA-LeRC) to perform soot volume fraction measurements for droplets using the Glovebox facility.

f) The PI was at Lewis during the summer of 1994 working with Dr. Randy Vander Wal using laser-Induced Incandescense for performing soot volume fraction measurements in droplet combustion. (results were presented by RVW at the Eastern States Sectional Meeting of the Combustion Institute, 1994).

5.0 FUTURE WORK

a) Perform soot volume fraction/temperature measurements under normal-gravity for test conditions outlined in section 2.

b) Incorporate optical diagnostic apparatus on the droplet combustion apparatus (that is being built at NASA-LeRC) for use in 2.2 sec droptower and aboard the DC-9. Reduced-gravity droplet combustion experiments for soot volume fraction and temperature measurements are scheduled for mid-summer, 1995.

c) Collaborate with Princeton researchers in incorporating revised thermophoretic models to calculate sootshell location.

d) Determine soot extinction constants for various fuels to be used in soot volume fraction experiments.

6.0 ACKNOWLEDGEMENTS

The authors gratefully acknowledge helpful advice regarding the implementation of a full-field light extinction technique provided by Mr. P. Greenberg, Dr. D. Griffin, Mr. B. Whiteside and Dr. D. Urban of NASA-LeRC. We would also like to thank Professor F.L. Dryer of Princeton, Professor F.A. Williams of UCSD, Dr. R. Vander Wal, Dr. P. Ferkul, Mr. D. Schultz and Dr. M. Vedha-Nayagem of NASA-LeRC and Drs. A. Hamins, T. Kashiwagi and C. Shaddix of NIST for helpful discussions regarding the work. This work was supported by NASA-LeRC through grant #NAG3-1631. Kirk Jensen would like to acknowledge support from the AMOCO Foundation Fellowship.

7.0 REFERENCES

1. Kumagai, S. and Isoda, H., Sixth Symposium (Int'l) on Combustion, p. 139. (1957).
2. Kumagai, S., Sakai, T. and Okajima, S., Thirteenth Symposium (Int'l) on Combustion, p. 779 (1971).
3. Knight, B. and Williams, F.A., Combustion and Flame, 38:111 (1980).
4. Shaw, B.D., Dryer, F.L., Williams, F.A. and Haggard, J.B., Jr., Acta Astronautica, 17:1195 (1988).
5. Choi, M.Y., Dryer, F.L., and Haggard, J.B., Twenty-Third Symposium (Int'l) on Combustion, The Combustion Institute, Pittsburgh, PA., p.1597 (1990).
6. Jackson, G.S., Avedisian, C.T. and Yang, J.C., Proc. R. Soc. Lond A, 435:359 (1991).
7. Avedisian, C.T., "Droplet Combustion and Soot Formation in Microgravity", Eastern States Section of the Combustion Institute, Clearwater Beach, FL (1994).
8. Vranos, A. and Liscinsky, D.S., Combustion Sci. Tech., 38:145 (1984).
9. Chung, S.H. and Law, C.K., Combustion and Flame, 64:237 (1986).
10. Williams, F.A. and Dryer, F.L., Science Requirements Document for Droplet Combustion Experiment, 1994.
11. Chao, B.H., Law, C.K. and T'ien, J.S., Twenty-Third Symposium (Int'l) on Combustion, The Combustion Institute, Pittsburgh, PA., p.523 (1990).
12. Grosshandler, W.L., RADCAL: A Narrow Band Model for Radiation Calculation in a Combustion Environment, NIST Technical Note 1402 (1992).
13. Yang, J.C. and Avedisian, C.T., Twenty-Second Sumposium (Int'l) on Combustion, The Combustion Institute, p. 2037 (1988).
14. Hara, H. and Kumagai, S., Twenty-Third Symposium (Int'l) on Combustion, The Combustion Institute, p. 1605 (1990).
15. Shaw, B.D. and Williams, F.A., Int. J. of Heat and Mass Transfer, 33:301 (1990).
16. Friedlander, S.K., Smoke, Dust and Haze, Wiley and Sons, N.Y., (1977).
17. Waldmann, L. and Schmitt, K.H., Thermophoresisn and Diffusiophoresis of Aerosols, Chap VI in Aerosol Science (C.N. Davies, ed.), Academic, N.Y., (1966)
18. Talbot. L. and Cheng, R.K., Schefer, R.W. and Willis, D.R., J. Fluid Mech. 101:737 (1980).
19. Choi, M.Y., Dryer, F.L., Green, G.J. and Sangiovanni, J.J., AIAA Paper 93-0823 (1993).
20. Kadota, T. and Hiroyasu, H., Comb. Flame, 55:195 (1984).
21. Griffin, D.W. and Greenberg, P.S., "Selected Microgravity Combustion Diagnostics Techniques", 2nd Int'l Microgravity Combustion Workshop Proceedings, Sept. 1992.
22. Greenberg, P.S. and Ku, J.C., "Soot Volume Fraction Imaging", Applied Optics, submitted, 1995.
23. Santoro, R.J., Semerjian, H.G., and Dobbins, R.A., Combust. Flame 51:203 (1983).

24. Dasch, C.J., Applied Optics, 31:146 (1992).
25. Sunderland, P.B., Koylu, U.O. and Faeth, G.M., Combust and flame, 110:310 (1995).
26. Zhou, Z. and Choi, M.Y., "Measurement of Dimensionless Extinction Constant of Soot Generated Usng Various Fuels", To be presented at the Central/Western/Mexican Sections of the Combustion Institute, San Antonio, TX, April, 1995.
27. Faeth, G.M., Science Requirements Document for Laminar Soot Processes Experiment, 1994.
28. Köylü, Ü.Ö. and Faeth, G.M., J. Heat Transfer, 115:409 (1993).
29. Sivathanu, Y.R. and Faeth, G.M., Combstion and Flame, 81:150 (1990).
30. Megaridis, C.M. and Dobbins, R.A., Twenty-Second Symposium (Int'l) on Combustion, p. 353, 1988.
31. Choi, M.Y. and Zhou, Z., Digital Image Processing Algorithm for the Measurement of Soot Radius of Gyration, in progress, 1995.

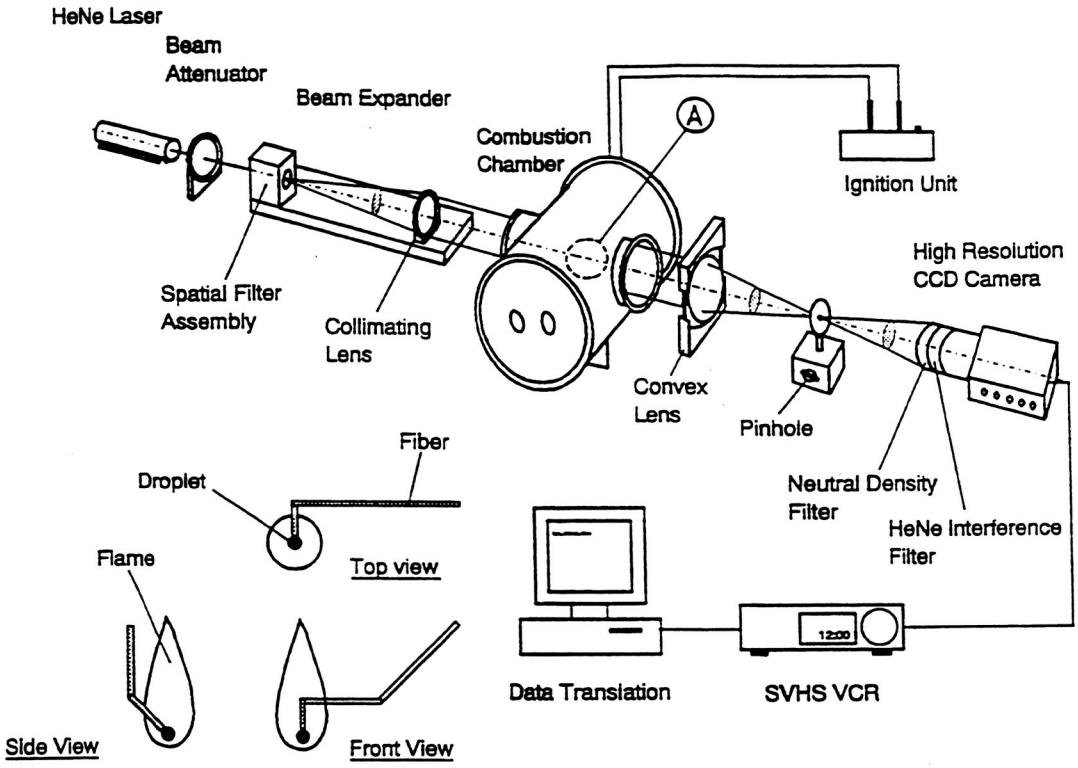

Figure1

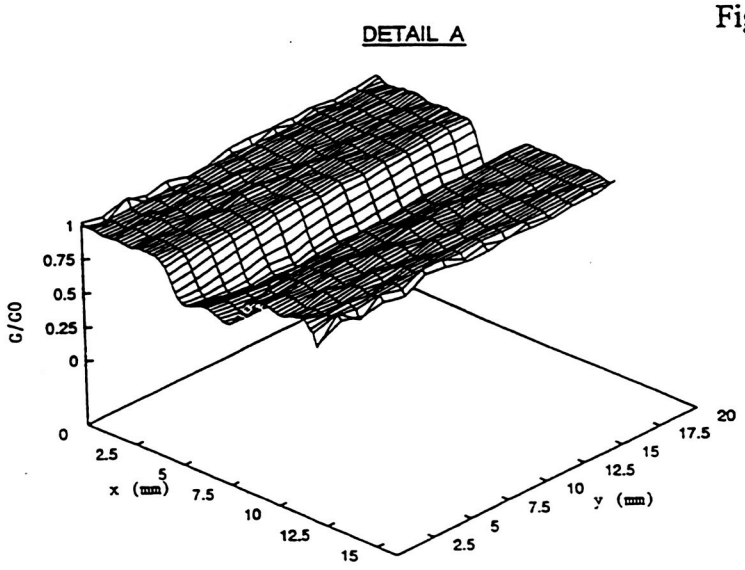

Figure 2

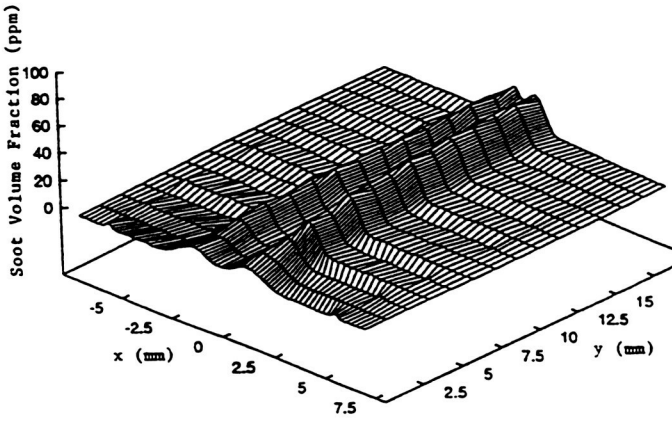

Figure 3